



Contents lists available at ScienceDirect

## Arabian Journal of Chemistry

journal homepage: [www.ksu.edu.sa](http://www.ksu.edu.sa)

Original article

Investigating the preparation process of excellent  $\text{Cu}_3\text{VSe}_4$  absorption layer prepared by amine-thiol systemYanqing Liu<sup>a,c</sup>, Yanchun Yang<sup>a,b,c,\*</sup>, Juntong Ren<sup>a,c</sup>, Guonan Cui<sup>a,c</sup>, Xin Zhao<sup>a,c</sup>, Rui Wang<sup>a,c</sup>, Lulu Bai<sup>a,c</sup>, Chengjun Zhu<sup>b,\*\*</sup><sup>a</sup> School of Physics and Electronic Information, Inner Mongolia Key Laboratory for Physics and Chemistry of Functional Materials, Inner Mongolia Normal University, 81 Zhaowuda Road, Huhhot, Inner Mongolia 010022, China<sup>b</sup> School of Physical Science and Technology, Inner Mongolia University, 2352 West University Road, Huhhot, Inner Mongolia 010021, China<sup>c</sup> Inner Mongolia Autonomous Region Engineering Research Center for Rare Earth Functions and New Energy Storage Materials, Inner Mongolia Normal University, 81 Zhaowuda Road, Huhhot, Inner Mongolia 010022, China

## ARTICLE INFO

## Keywords:

$\text{Cu}_3\text{VSe}_4$  thin films  
Amine-thiol method  
Cu/V ratio  
Selenization conditions

## ABSTRACT

$\text{Cu}_3\text{VSe}_4$  material has become a new kind of photovoltaic absorber due to its optical bandgap matching light-absorbing, abundant elements in crust, and high light absorption coefficient. Here, we prepared  $\text{Cu}_3\text{VSe}_4$  thin films by amine-thiol method and investigated the preparation process of excellent  $\text{Cu}_3\text{VSe}_4$  absorption layer for the first time. The effects of various Cu/V ratios on the morphology, structure, and electrical properties of the films are studied. XRD and Raman results show that pure-phase  $\text{Cu}_3\text{VSe}_4$  films are obtained with the Cu/V ratios lower than 2.9. SEM results simply adjusting the Cu/V ratio cannot obtain a compact selenized  $\text{Cu}_3\text{VSe}_4$  thin films. The best crystallinity of thin film with 2.8 of Cu/V ratio is named as  $\text{Cu}_{2.8}\text{VSe}_4$  and selected as the representative. Though optimizing the selenization conditions, a dense morphology and good electrical properties of the absorption layer can be prepared under 570 °C of the high-temperature process. Our findings can lay the favorable foundation for high-efficiency  $\text{Cu}_3\text{VSe}_4$  devices.

## 1. Introduction

Because they possess the adjustable optical bandgaps and excellent stability, the copper-based thin film solar cells have been rapidly developed and have become an important option for renewable energy. Among these thin film solar cells, CdTe,  $\text{Cu}(\text{In,Ga})\text{Se}_2$ , and  $\text{Cu}_2\text{ZnSn}(\text{S,Se})_4$  materials are representative and have also made great progress (Kurley et al., 2017; Nakamura et al., 2019; Yang et al., 2024). However, the scarce In, Ga and Te elements, and the highly toxic Cd element, have become the restricting CdTe and  $\text{Cu}(\text{In,Ga})\text{Se}_2$  developments (Wang et al., 2020). High harmful defects density is also main limitation of  $\text{Cu}_2\text{ZnSn}(\text{S,Se})_4$  solar cells. The new copper-based photovoltaic materials need to be developed. Recently, the ternary copper-based  $\text{Cu}_3\text{MCh}_4$  ( $\text{M} = \text{V, Nb, Ta}$ ;  $\text{Ch} = \text{S, Se, Te}$ ) semiconductor materials have been reported, and they have been confirmed as p-type semiconductors (Kehoe et al., 2015).  $\text{Cu}_3\text{VS}_4$  and  $\text{Cu}_3\text{VSe}_4$  materials have the optical bandgap matching with sunlight and be regarded as the absorption layer

of photovoltaic devices. At present, there are a few reports of  $\text{Cu}_3\text{VS}_4$  thin film (Mantella et al., 2018; Wen et al., 2021;), but few reports of  $\text{Cu}_3\text{VSe}_4$  thin film. Liu et al. fabricated  $\text{Cu}_3\text{VSe}_4$  nanocrystal and  $\text{Cu}_3\text{VSe}_4$ -FTO thin films with p-type characteristic and photocurrent of  $\sim 4 \mu\text{A}/\text{cm}^2$  (Liu et al., 2020). Afterward, they reported the preparation process and properties of  $\text{Cu}_3\text{VSe}_4$  nanosheets (Liu et al., 2020). Wu et al. prepared  $\text{Cu}_3\text{VSe}_4$  nanocrystal by one-pot reaction in oil phase (Wu et al., 2022). Nano-structural  $\text{Cu}_3\text{VSe}_4$  synthesis needs usually the long-chain ligand which is not friendly to the optoelectronic devices. Therefore, for the future photovoltaic applications, the preparation process of  $\text{Cu}_3\text{VSe}_4$  thin films need be studied.

With the advantages of controlling the elemental ratios accurately, low cost, and simplicity of large-area preparation, the precursor solution approach is a particularly ideal process for the development and manufacture of thin-film solar cells (Qin et al., 2022; Zhang et al., 2019). And the commonly used precursor solution systems include DMSO (Ki and Hillhouse, 2011; Gong et al., 2020; Xin et al., 2015), DMF (Liu et al.,

\* Corresponding author at: School of Physics and Electronic Information, Inner Mongolia Key Laboratory for Physics and Chemistry of Functional Materials, Inner Mongolia Normal University, 81 Zhaowuda Road, Huhhot, Inner Mongolia 010022, China.

\*\* Corresponding author.

E-mail addresses: [20170020@imnu.edu](mailto:20170020@imnu.edu) (Y. Yang), [cjzhu@imu.edu.cn](mailto:cjzhu@imu.edu.cn) (C. Zhu).

<https://doi.org/10.1016/j.arabjc.2024.105839>

Received 26 February 2024; Accepted 16 May 2024

Available online 19 May 2024

1878-5352/© 2024 The Authors. Published by Elsevier B.V. on behalf of King Saud University. This is an open access article under the CC BY-NC-ND license (<http://creativecommons.org/licenses/by-nc-nd/4.0/>).

2015; Luan et al., 2019; Collord and Hillhouse, 2016), amine-thiol (Fu et al., 2018; Tian et al., 2018), MOE (Zhao et al., 2021) etc., here, the amine-thiol system is used to prepare the thin films. It is well known that amine-thiol system can dissolve the elemental metal, metal oxide, metal salt, elemental S, elemental Se powders, and so on (Zhao et al., 2021; Fu et al., 2016; McCarthy et al., 2015). Yang et al. prepared the pure  $\text{Cu}_2\text{ZnSnSe}_4$  thin film solar cells by amine-thiol system (Yang et al., 2016). Therefore, the amine-thiol system is very suitable for solution-processed  $\text{Cu}_3\text{VSe}_4$  thin films. High performance solar cells often require the dense absorption layer with the pure phase, low density of harmful defects, and high crystallinity. Whether  $\text{Cu}_3\text{VSe}_4$  thin films prepared by the amine-thiol system can be used as the absorption layer of solar cells or not, their preparation process needs to be studied and optimized.

In this study, based on the thiol-amine solution system, through tuning the Cu/V feeding ratio in the precursor solutions,  $\text{Cu}_3\text{VSe}_4$  thin films with various Cu/V ratios could be prepared, and their properties were also investigated. The optimal crystallinity of thin film with 2.8 of Cu/V ratio was confirmed. Based on this finding, further investigation was conducted to explore the influence of selenization conditions on the properties of  $\text{Cu}_3\text{VSe}_4$  thin films.

## 2. Experimental sections

### 2.1. $\text{Cu}_3\text{VSe}_4$ precursor solution preparation

Learned from our previous work of  $\text{Cu}_2\text{ZnSn(S,Se)}_4$  thin films (Yang et al., 2015),  $\text{Cu}_3\text{VSe}_4$  precursor solution was prepared as followed: 2 mL of thioglycolic acid and 3 mL of ethanolamine were placed in a 25 mL of conical flask and fully mixed under stirring on 70 °C hot plate. Next, 1 mmol  $\text{C}_{10}\text{H}_{14}\text{O}_5\text{V}$  and 3 mmol  $\text{C}_4\text{H}_6\text{CuO}_4\cdot\text{H}_2\text{O}$  were dissolved into this solution under stirring at 100 °C for 60 min until they were completely dissolved in this solution. After that, 300 mg Se powder was added under stirring for 30 min at 70 °C. The obtained viscous solution was cooled to room temperature. Finally, 7 mL of  $\text{C}_3\text{H}_8\text{O}_2$  was added under stirring for 30 min at 0 °C, forming the clean  $\text{Cu}_3\text{VSe}_4$  precursor solution with 3.0 of Cu/V ratio. By adjusting the amount of  $\text{C}_4\text{H}_6\text{CuO}_4\cdot\text{H}_2\text{O}$ , the precursor solutions with different Cu/V ratios were formed.

### 2.2. $\text{Cu}_3\text{VSe}_4$ thin films preparation

The  $\text{Cu}_3\text{VSe}_4$  precursor solutions with various Cu/V ratios were spin-coated on the Mo-sputtered soda-lime glass with 3900 rpm for 40 s, which was annealed on 320 °C for 1.5 min. This step repeated five times to obtain the as-deposited  $\text{Cu}_3\text{VSe}_4$  thin films with different Cu/V ratios. Finally, as-prepared  $\text{Cu}_3\text{VSe}_4$  thin films were selenized by two-step selenization processes. These selenization processes consisted of the same low-temperature condition (400 °C, 10 min) and the different high-temperature conditions (550 °C, 30 min; 560 °C, 30 min; 570 °C, 30 min; 580 °C, 30 min).

### 2.3. Characterization

The phase purity was achieved by X-ray diffraction (XRD) and Raman spectra. XRD pattern of thin films was measured on Empyrean powder, and Raman spectra was recorded on a HORIBA LabRAM ARAMIS. The micro-morphology was collected using scanning electron microscopy (SEM, Hitachi SU4800) and atomic force microscope (AFM, C-ypher.). The compositions of thin films were characterized by Energy dispersive spectrometry (EDS, built on the SEM). Average surface current was acquired using the conductive atomic force microscope (c-AFM) with a bias voltage of 2 V. Valence state was detected using the X-ray photoelectron spectroscopy (XPS) by a Thermo CIENTIFIC Nexsa.

## 3. Results and discussion

The absorption layer prepared by thiol-amine solution system usually involves two steps. Firstly, the as-deposited thin films are prepared by spin-coating precursor solution, and then the as-deposited thin films are selenized in high-temperature rapid thermal processing furnace to obtain absorption layer. Note that the extra Se needs be introduced in the selenization process, which is intended to provide the sufficient selenium vapor to promote the grain growth process and obtain a well-crystallized film. Here, the as-deposited  $\text{Cu}_3\text{VSe}_4$  thin films prepared by thiol-amine solution system are nanostructured and porous, with a thickness of approximately 0.99  $\mu\text{m}$  (Fig. S1 and 2). By adjusting the feed ratios of Cu and V sources, the  $\text{Cu}_3\text{VSe}_4$  precursor solutions with different Cu/V ratios were prepared, and the corresponding as-deposited  $\text{Cu}_3\text{VSe}_4$  thin films were also obtained by spin-coating these precursor solutions. Learned from  $\text{Cu}_2\text{ZnSn(S,Se)}_4$  thin films' experimental experiences, two-step selenization process is helpful for the crystallinity of the absorber, so all  $\text{Cu}_3\text{VSe}_4$  thin films with various Cu/V ratios could be selenized by the same two-step selenization process (Yin et al., 2022; Ren et al., 2020; Mi et al., 2022). The Cu/V ratio in films is observed to increase proportionally with the increasing Cu/V ratio in precursor solution (Fig. 1a). Fig. 1(b) shows XRD patterns of the selenized  $\text{Cu}_3\text{VSe}_4$  thin films with various Cu/V ratios. All films present the same diffraction peaks at 15.9°, 27.7°, 36.1°, 46.1°, and 54.7°, which can correspond to the (100), (111), (210), (220), and (311) planes, respectively, and exhibit the standard cubic structure. When the ratio of Cu/V is over 2.8, the diffraction peaks of  $\text{Cu}_2\text{S}$  appear. In order to further validate the phase purity of  $\text{Cu}_3\text{VSe}_4$  films, Raman spectra measurement can be used, as shown in Fig. S3. All samples have the vibration peaks at around 127, 149, 175, 210, 253, and 337  $\text{cm}^{-1}$  which belong to the  $\text{Cu}_3\text{VSe}_4$  phase, and no impure phase is observed, which is consistent with the reported literature (Zhai et al., 2023). Therefore, the pure phase of  $\text{Cu}_3\text{VSe}_4$  films needs to control the Cu/V ratio is less than 2.9.

In order to investigate the morphology of  $\text{Cu}_3\text{VSe}_4$  films with various Cu/V ratios, SEM measurement is carried out to elevate the morphology of all samples as shown in Fig. 2. When the feeding ratio of Cu/V is relatively small (~2.6), the enlarged grains are dispersed on the surface of the selenized  $\text{Cu}_3\text{VSe}_4$  thin films, resulting in a low coverage. As the feeding ratio of Cu/V increases, the coverage of the film increases and the film begins to become dense. The selenized  $\text{Cu}_3\text{VSe}_4$  thin films present the best compactness until the Cu/V ratio is 2.8, and the impure phase (as circled in red) can appear with 3.0 of Cu/V ratio. The region circled in red can be observed to present a hexagonal phase which is consistent with the reported  $\text{Cu}_2\text{S}$  phase (Sigman et al., 2003). Besides, the diffraction peaks of  $\text{Cu}_2\text{S}$  phase can be detected in XRD patterns. Therefore, the region circled in red thought to be  $\text{Cu}_2\text{S}$  phase. The presence of impure phase is fatal to high-quality absorption layers. The selenized  $\text{Cu}_3\text{VSe}_4$  thin films with Cu/V ratio higher than 2.9 are not suitable as candidates for high-quality absorption layers. Meanwhile, the low coverage of the films with 2.6 of Cu/V ratio is also not considered further. So, the selenized  $\text{Cu}_3\text{VSe}_4$  thin films with Cu/V ratio of 2.75 and 2.85 are supplemented. Fig. 3 and Fig. S4 show XRD patterns and SEM images of these selenized  $\text{Cu}_3\text{VSe}_4$  thin films. All diffraction peaks are coincident with the above samples' ones, and can belong to (100), (111), (210), (220), and (311) planes, respectively. Based on our experiment experience, (100) is dominant orientation in the  $\text{Cu}_3\text{VSe}_4$  crystal growth, so the corresponding enlarged (100) peaks can be observed in Fig. 3b. The crystallinity of films can possess the optimal with 2.8 of Cu/V ratio, but the compactness of all films is still poor. And there appears to be a little peak shift, which is attributed to the enlarged grain. These conclusions indicate the Cu/V ratio has little impact on the compactness of selenized  $\text{Cu}_3\text{VSe}_4$  films.

The electrical properties of microscopic dense regions in above films are studied and depicted in Fig. 4. The chose scanning region is 3 × 3  $\mu\text{m}^2$ . The average surface roughness of the samples is calculated, as shown in Fig. S5. A decreased average surface roughness can be from

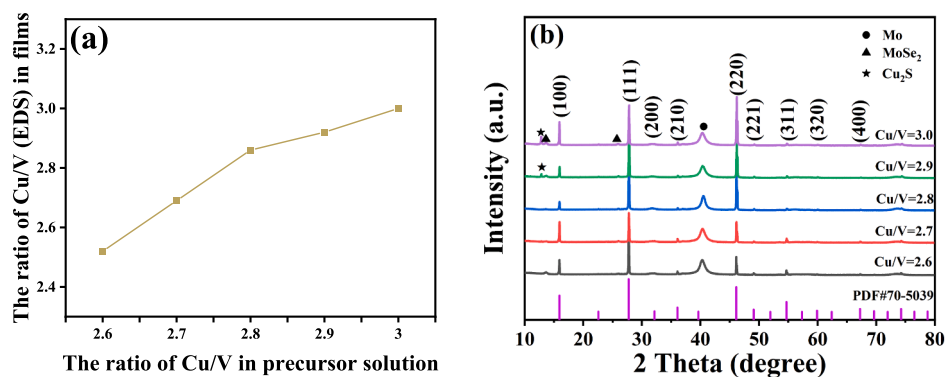


Fig. 1. (a) Relationship Cu/V ratios in films with the feeding ratio of Cu/V in precursor solution and (b) XRD patterns of the selenized  $\text{Cu}_3\text{VSe}_4$  films with various Cu/V ratios.

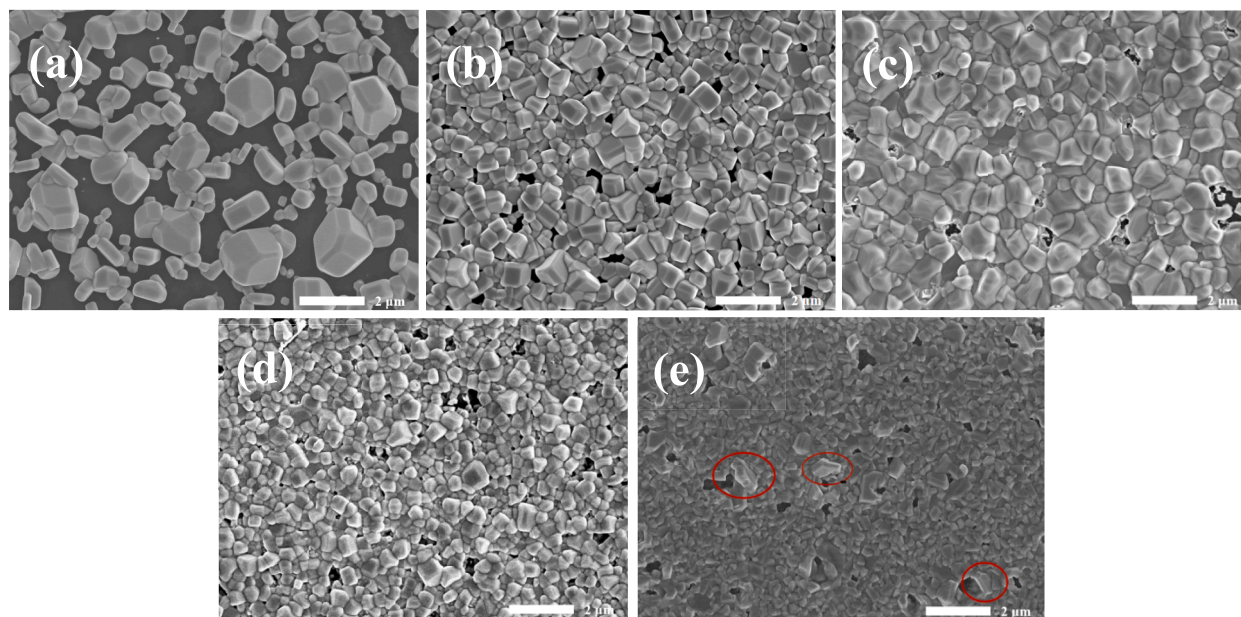


Fig. 2. SEM images of  $\text{Cu}_3\text{VSe}_4$  films with the various Cu/V ratios. (a) 2.6, (b) 2.7, (c) 2.8, (d) 2.9, (e) 3.0.

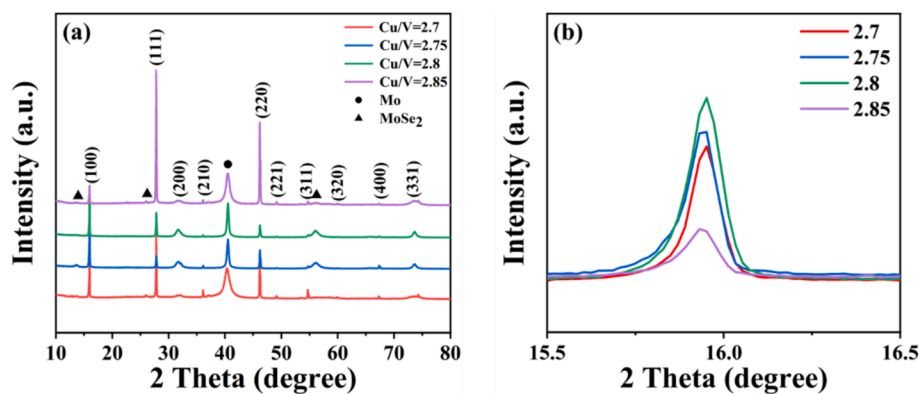


Fig. 3. (a) XRD patterns of the selenized  $\text{Cu}_3\text{VSe}_4$  thin films with various Cu/V ratios and (b) the corresponding enlarged (100) peaks.

96.7 nm to 68.6 nm, with the increasing ratio of Cu/V, which should stem from the improved coverage of films. Afterwards, 2 V bias voltage is applied to observe the surface current distribution in the films. It can be seen that the sample with 2.8 of Cu/V ratio has the most and clearest current distribution, and its average current can reach 1.55nA, which

indicates that it has the best carrier transport performance. All results show  $\text{Cu}_3\text{VSe}_4$  thin films with 2.8 of Cu/V ratio are valuable for the absorption layers, and their properties are worth studying. And  $\text{Cu}_3\text{VSe}_4$  thin films with 2.8 of Cu/V ratio are named as  $\text{Cu}_{2.8}\text{VSe}_4$  thin films.

The primary factor for the outstanding absorption layer is a dense

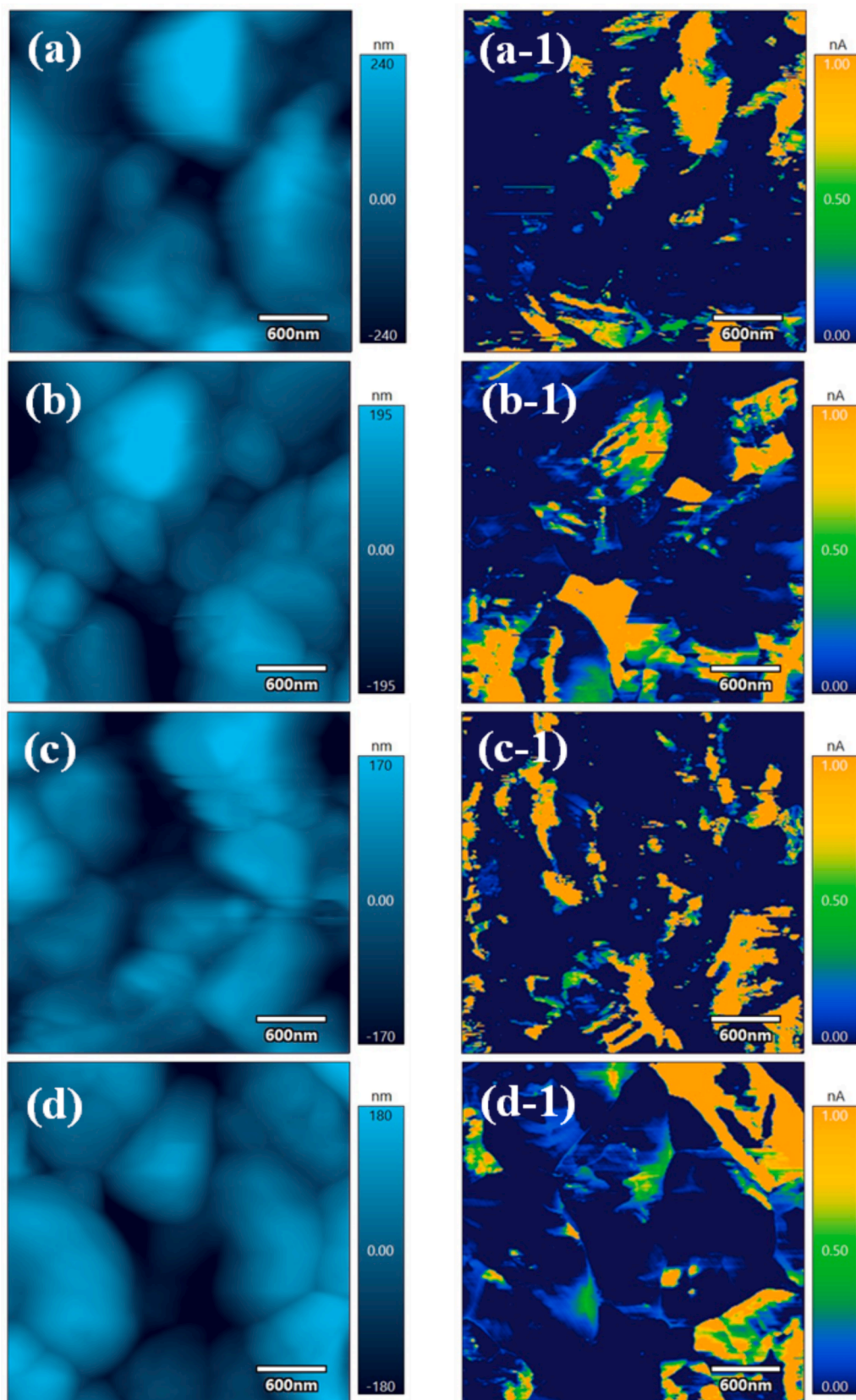


Fig. 4. AFM and c-AFM images of the selenized  $\text{Cu}_3\text{VSe}_4$  films with the various Cu/V ratios. (a, a-1) 2.7, (b, b-1) 2.75, (c, c-1) 2.8, (d, d-1) 2.85.

thin film, and the selenization process of the  $\text{Cu}_{2.8}\text{VSe}_4$  thin films also needs to be further optimized. Here, our selenization process is the two-step selenization method, and its high-temperature process is known to be closely related to the compactness of the film. Therefore, we optimized the high-temperature selenization (HT) process of the  $\text{Cu}_{2.8}\text{VSe}_4$  film. Based on our experiment experience (Ren et al., 2024), the optimal selenization time of  $\text{Cu}_3\text{V}(\text{S},\text{Se})_4$  films is confirmed at 30 min, so the selenization time of the  $\text{Cu}_{2.8}\text{VSe}_4$  film is also selected as 30 min. Fig. 5 shows SEM images of films with the different temperatures of HT process. As the temperature of HT process increases, the crystal size increases, the compactness of  $\text{Cu}_{2.8}\text{VSe}_4$  films improves, and the large-grain layer thickens. Under the selenization condition of  $570^\circ\text{C}$ , the film becomes completely dense, meeting the basic requirement of a high-quality absorption layer. And the corresponding XRD patterns

(Fig. 6) are used to assess the phase purity and crystal structure of  $\text{Cu}_{2.8}\text{VSe}_4$  film. Except for Mo peak, all peaks can be attributed to  $\text{Cu}_3\text{VSe}_4$  phase, proving that all films are pure phases. The same peak positions demonstrate the temperature of HT process affects a little the crystal structure of  $\text{Cu}_{2.8}\text{VSe}_4$  film, but has the significant impact on the crystallinity of  $\text{Cu}_{2.8}\text{VSe}_4$  film. According to half-high width of diffraction patterns (Table S1), An increased average crystal size of  $\text{Cu}_{2.8}\text{VSe}_4$  film is obtained with the increased selenization temperature, which is similar to that observed under SEM. And  $\text{Cu}_{2.8}\text{VSe}_4$  film with the HT temperature of  $570^\circ\text{C}$  is defined as the best sample. Besides, the valence states of main elements in the best sample are also studied, as shown in Fig. S6. The peak of Cu 2p appears at 932.7 and 952.5 eV, and the maximum split value is 19.8 eV (Mohammadnezhad et al., 2020; Zhang et al., 2020). The peak of V 2p is located at 513.9 eV and 521.6 eV, with

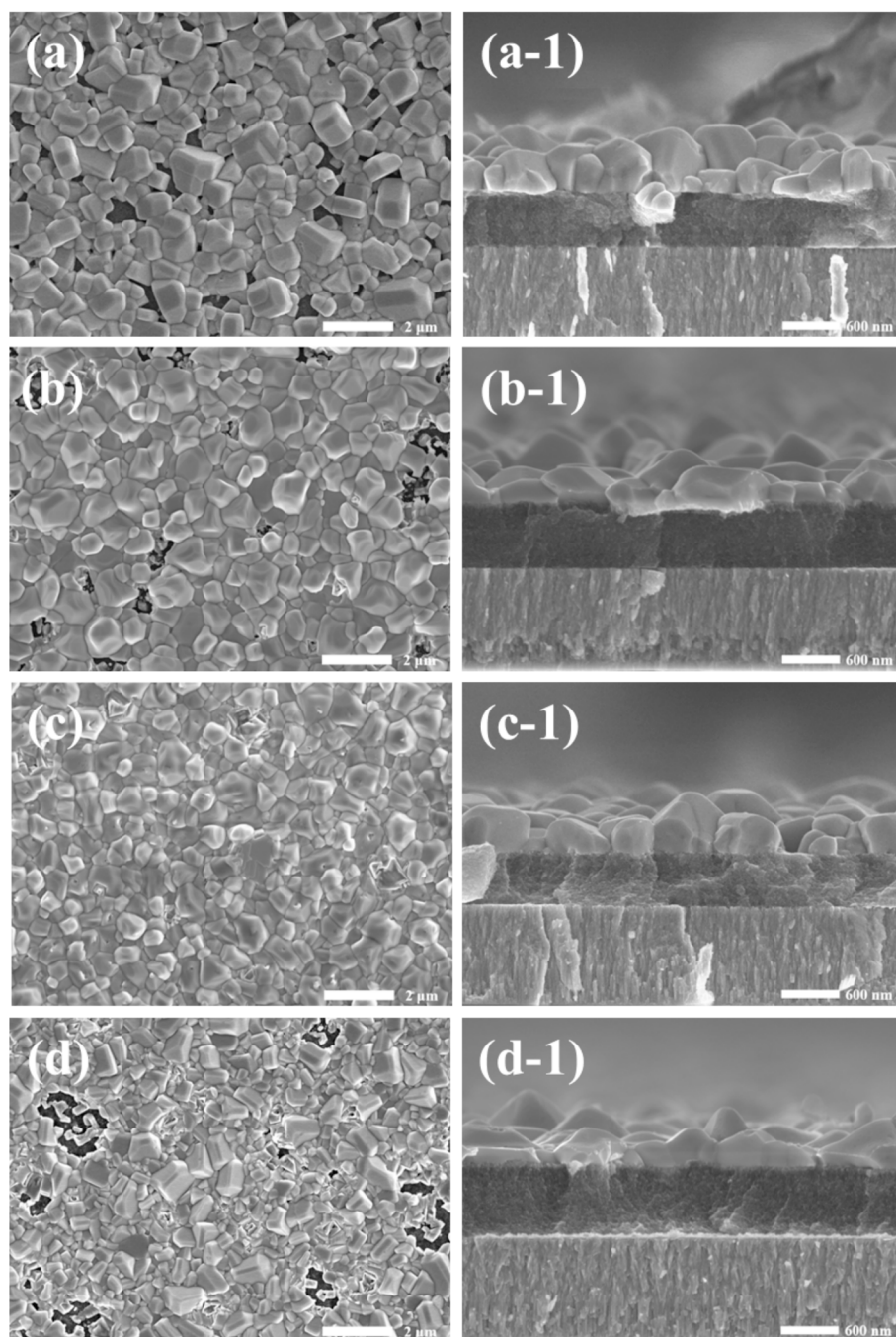


Fig. 5. SEM images of  $\text{Cu}_{2.8}\text{VSe}_4$  films with the different temperatures of HT process. (a, a-1)  $550^\circ\text{C}$ , (b, b-1)  $560^\circ\text{C}$ , (c, c-1)  $570^\circ\text{C}$ , (d, d-1)  $580^\circ\text{C}$ .

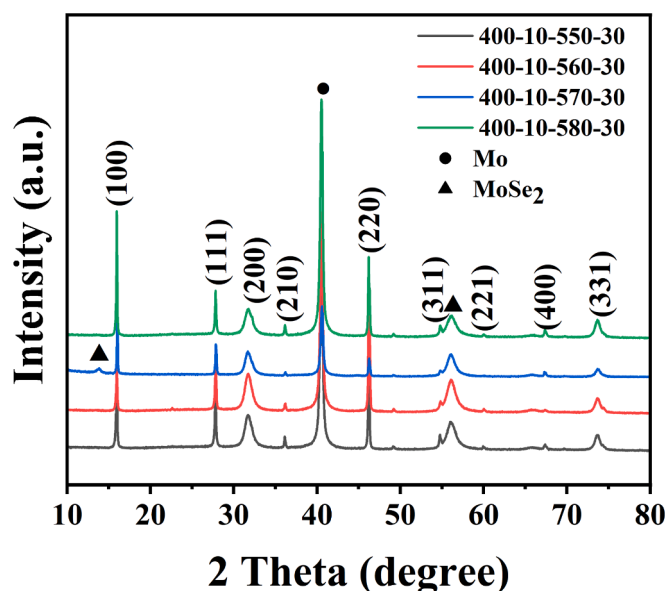


Fig. 6. XRD patterns of  $\text{Cu}_{2.8}\text{VSe}_4$  films with the different temperatures of HT process.

the maximum split value of 7.7 eV (Liu et al., 2020). Se 3d peak is located at 54.1 eV and 55.2 eV, and the split value is 1.1 eV (Xue et al., 2021). These split values correspond to  $\text{Cu}^+$ ,  $\text{V}^{5+}$ , and  $\text{Se}^{2-}$ , respectively.

Fig. 7 shows the other properties (AFM, c-AFM images, absorption spectrum and Tauc curve) of the best sample. AFM and c-AFM images (Fig. 7a and b) show the best sample present the nice topography and low average surface roughness ( $\sim 51.516$  nm), and the average surface current can be improved to 1.974 nA. The absorption characteristic of the best film is assessed in Fig. 7c. There are three peaks located at around 435, 500, and 624 nm, respectively, which indicates the signature of the nanoscale sylvanites  $\text{Cu}_3\text{VSe}_4$  phase. When converting wavelength in photo energy, these three absorption bands correspond to 3.17 eV, 2.20 eV and 1.83 eV which are in accordance with bandgap of VB-CB, VB-IB I, and VB-IB II, respectively (Oguchi et al., 1980; Bastola et al., 2018). This result shows the prepared  $\text{Cu}_{2.8}\text{VSe}_4$  material possesses the intermediate bandgap. And there are two tuning points at 1.76 and 2.23 eV in the Tauc curve, which indicates further the intermediate band of  $\text{Cu}_{2.8}\text{VSe}_4$  sample. These results demonstrate  $\text{Cu}_{2.8}\text{VSe}_4$  film with the HT temperature of 570 °C can be regarded as the absorption layer of photovoltaic devices.

#### 4. Conclusion

In summary,  $\text{Cu}_3\text{VSe}_4$  thin films were prepared by thiol-amine solution system for the first time, and the preparation process of the excellent  $\text{Cu}_3\text{VSe}_4$  absorption layer was also studied. The feeding ratio of

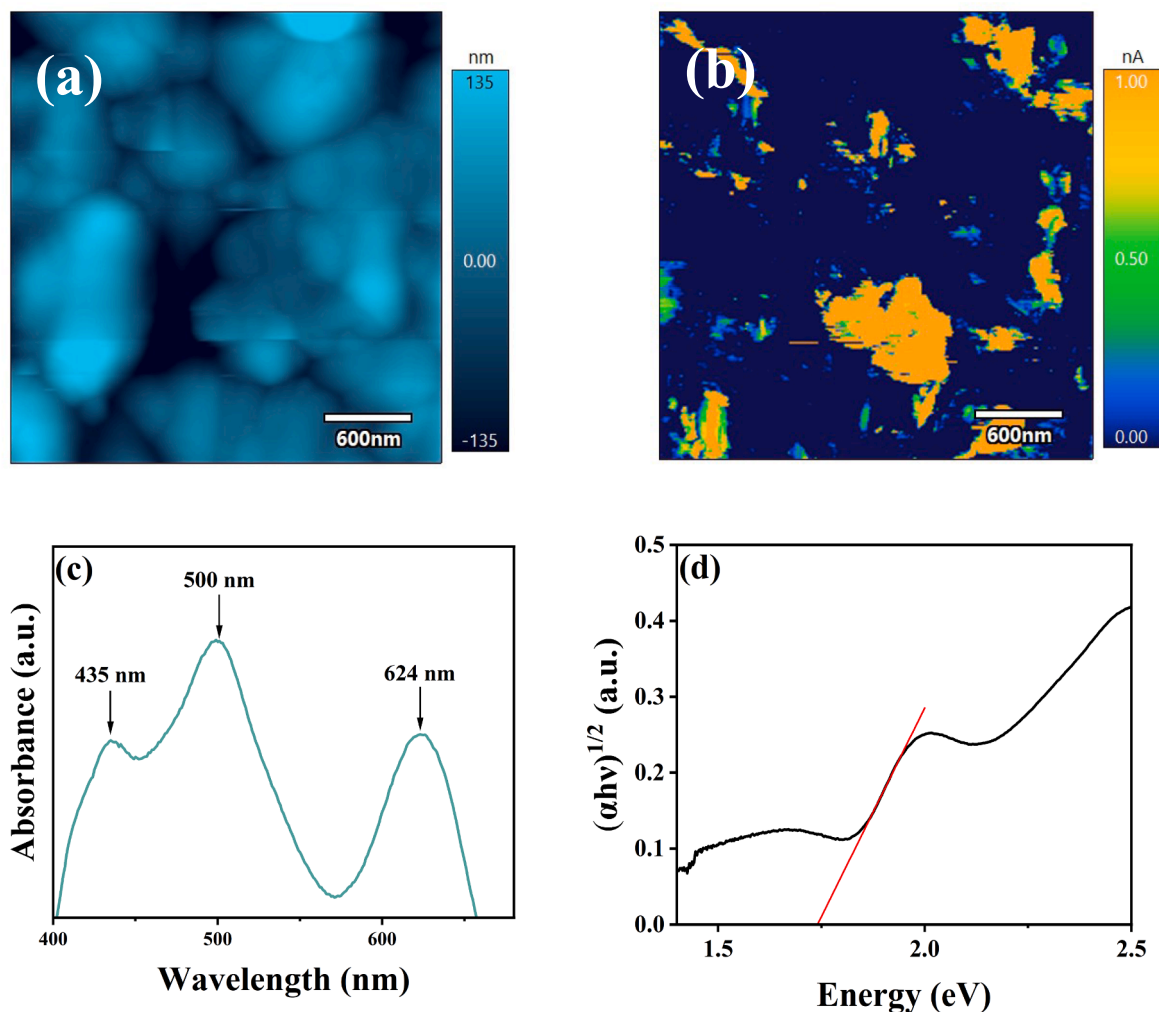


Fig. 7. The other properties of the best sample. (a) AFM image, (b) c-AFM image, (c) absorption spectrum, (d) Tauc curve.

Cu/V need be controlled below 2.9 to obtain pure phase  $\text{Cu}_3\text{VSe}_4$  films, but it has little effect on the compactness of the films. And the reasonable properties of films with 2.8 of Cu/V ratio (named as  $\text{Cu}_{2.8}\text{VSe}_4$  film) can present the potential candidate of absorption layer. Based on  $\text{Cu}_{2.8}\text{VSe}_4$  film, by further optimizing the selenization process of the films, the pure phase, compact, and benign electrical properties of  $\text{Cu}_{2.8}\text{VSe}_4$  absorption layer films can be achieved under 570 °C of the high-temperature process, which is suitable for the photovoltaic devices.

### CRedit authorship contribution statement

**Yanqing Liu:** Conceptualization, Data curation, Formal analysis, Investigation, Methodology, Validation, Writing – original draft. **Yanchun Yang:** Funding acquisition, Project administration, Resources, Supervision, Writing – review & editing. **Junting Ren:** Investigation, Visualization. **Guonan Cui:** Resources, Visualization. **Xin Zhao:** Visualization. **Rui Wang:** Investigation, Visualization. **Lulu Bai:** Visualization. **Chengjun Zhu:** Funding acquisition, Supervision.

### Declaration of competing interest

The authors declare that they have no known competing financial interests or personal relationships that could have appeared to influence the work reported in this paper.

### Acknowledgements

This work was supported by National Natural Science Foundation of China (Grant No. 62164010, 61804085, and 62064010), China Postdoctoral Science Foundation (Grant No. 2019M653806XB).

### Appendix A. Supplementary data

XRD pattern, SEM surface and cross-sectional images of as-deposited  $\text{Cu}_3\text{VSe}_4$  thin films. Raman spectra of the selenized  $\text{Cu}_3\text{VSe}_4$  films with the various Cu/V ratios. Top view and cross-sectional SEM images of the selenized  $\text{Cu}_3\text{VSe}_4$  films with the various Cu/V ratios. The average surface roughness of the  $\text{Cu}_3\text{VSe}_4$  with the various Cu/V ratios. Half-high width of diffraction patterns of films with the different HT temperature. XPS spectra of the best sample. Supplementary data to this article can be found online at <https://doi.org/10.1016/j.arabjc.2024.105839>.

### References

- Bastola, E., Bhandari, K.P., Subedi, I., et al., 2018. Structural, optical, and hole transport properties of earth-abundant chalcopyrite ( $\text{CuFeS}_2$ ) nanocrystals. *MRS Commun* 8 (3), 970–978. <https://doi.org/10.1557/mrc.2018.117>.
- Collord, A.D., Hillhouse, H.W., 2016. Germanium alloyed kesterite solar cells with low voltage deficits. *Chem. Mater.* 28 (7), 2067–2073. <https://doi.org/10.1021/acs.chemmater.5b04806>.
- Fu, J., Tian, Q., Zhou, Z.J., Kou, D., et al., 2016. Improving the performance of solution-processed  $\text{Cu}_2\text{ZnSn}(\text{S}, \text{Se})_4$  photovoltaic materials by  $\text{Cd}^{2+}$  substitution. *Chem. Mater.* 28 (16), 5821–5828. <https://doi.org/10.1021/acs.chemmater.6b02111>.
- Fu, J., Fu, J., Tian, Q., Wang, H., et al., 2018. Tuning the Se content in  $\text{Cu}_2\text{ZnSn}(\text{S}, \text{Se})_4$  absorber to achieve 9.7 % solar cell efficiency from a thiol/amine-based solution process. *ACS Appl. Energy Mater.* 1 (2), 594–601. <https://doi.org/10.1021/acsaem.7b00146>.
- Gong, Y., Zhang, Y., Jedlicka, E., Giridharagopal, R., et al., 2020.  $\text{Sn}^{4+}$  precursor enables 12.4 % efficient kesterite solar cell from DMSO solution with open circuit voltage deficit below 0.30 V. *Sci. China Mater.* 64, 52–60. <https://doi.org/10.1007/s40843-020-1408-x>.
- Kehoe, A.B., Scanlon, D.O., Watson, G.W., 2015. The electronic structure of sulvanite structured semiconductors  $\text{Cu}_3\text{MCh}_4$  (M = V, Nb, Ta; Ch = S, Se, Te): prospects for optoelectronic applications. *J. Mater. Chem. C* 3, 12236–12244. <https://doi.org/10.1039/C5TC02760H>.
- Ki, W., Hillhouse, H.W., 2011. Earth-abundant element photovoltaics directly from soluble precursors with high yield using a non-toxic solvent. *Adv. Energy Mater.* 1 (5), 732–735. <https://doi.org/10.1002/aenm.201100140>.
- Kurley, J.M., Panthani, M.G., Crisp, R.W., et al., 2017. Transparent Ohmic contacts for solution-processed, Ultrathin CdTe. *ACS Energy Lett.* 2 (1) <https://doi.org/10.1021/acsenenergylett.6b00587>.

- Liu, M., Lai, C.Y., Selopal, G. S., Radu, D.R., 2020a. Synthesis and optoelectronic properties of  $\text{Cu}_3\text{VSe}_4$  nanocrystals. *PLoS One* 15 (5), e0232184. <https://doi.org/10.1371/journal.pone.0232184>.
- Liu, M., Lai, C.Y., Zhang, M., Radu, D.R., 2020b. Cascade synthesis and optoelectronic applications of intermediate bandgap  $\text{Cu}_3\text{VSe}_4$  nanosheets. *Sci. Rep.* 10 (1), 21679. <https://doi.org/10.1038/s41598-020-78649-9>.
- Liu, F., Shen, S., Zhou, F., Song, N., et al., 2015. Kesterite  $\text{Cu}_2\text{ZnSnS}_4$  thin film solar cells by a facile DMF-based solution coating process. *J. Mater. Chem. C* 3 (41), 10783–10792. <https://doi.org/10.1039/C5TC01750E>.
- Luan, H., Yao, B., Li, Y., Liu, R., et al., 2019. Influencing mechanism of cationic ratios on efficiency of  $\text{Cu}_2\text{ZnSn}(\text{S}, \text{Se})_4$  solar cells fabricated with DMF-based solution approach. *Sol. Energy Mater. Sol. Cells* 195, 55–62. <https://doi.org/10.1016/j.solmat.2019.02.029>.
- Mantella, V., Ninova, S., Saris, S., Louidice, A., et al., 2018. Synthesis and size-dependent optical properties of intermediate band gap  $\text{Cu}_3\text{VS}_4$  nanocrystals. *Chem. Mater.* 31 (2), 532–540. <https://doi.org/10.1021/acs.chemmater.8b04610>.
- McCarthy, C.L., Webber, D.H., Schueller, E.C., Brutchey, R.L., 2015. Solution-Phase conversion of bulk metal oxides to metal chalcogenides using a simple Thiol-Amine solvent mixture. *Angew. Chem. Int. Ed.* 54 (29), 8378–8381. <https://doi.org/10.1002/ange.201503353>.
- Mi, Y., Yang, Y., Cui, G., Ren, J., et al., 2022. Exploring the optimal two-step selenization process to enhance the performance of ionic liquid solution based  $\text{Cu}_2\text{ZnSn}(\text{S}, \text{Se})_4$  thin film solar cells. *J. Alloys Compd.* 909, 164740 <https://doi.org/10.1016/j.jallcom.2022.164740>.
- Mohammadnezhad, M., Liu, M., Selopal, G.S., Navarro-Pardo, F., et al., 2020. Synthesis of highly efficient  $\text{Cu}_2\text{ZnSnS}_x\text{Se}_{4-x}$ (CZTSSe) nanosheet electrocatalyst for dye-sensitized solar cells. *Electrochim. Acta* 340, 135954. <https://doi.org/10.1016/j.electacta.2020.135954>.
- Nakamura, M., Yamaguchi, K., Kimoto, Y., Yasaki, Y., et al., 2019. Cd-Free Cu(In, Ga)(Se, S)<sub>2</sub> thin-film solar cell with record efficiency of 23.35 %. *IEEE J. Photovolt.* 9 (6), 1863–1867. <https://doi.org/10.1109/JPHOTOV.2019.2937218>.
- Oguchi, T., Sato, K., Teranishi, T., 1980. Optical reflectivity spectrum of a  $\text{CuFeS}_2$  single crystal. *J. Phys. Soc. Jpn.* 48 (1), 123–128. <https://doi.org/10.1143/JPSJ.48.123>.
- Qin, X., Xu, B., Lin, J., Chen, J., et al., 2022. Above 10 % efficient electrodeposited  $\text{Cu}_2\text{ZnSn}(\text{S}, \text{Se})_4$  solar cell achieved by modifying precursor. *Sol. Energy Mater. Sol. Cells* 242, 111781. <https://doi.org/10.1016/j.solmat.2022.111781>.
- Ren, J., Yang, Y., Haschuloo, O., et al., 2024. Solution-processed  $\text{Cu}_3\text{V}(\text{S}, \text{Se})_4$  absorbers for thin films solar cells. *Ceram. Int.* <https://doi.org/10.1016/j.ceramint.2024.04.371>.
- Ren, G., Zhuang, D., Zhao, M., Wei, Y., et al., 2020. CZTSSe solar cell with an efficiency of 10.19 % based on absorbers with homogeneous composition and structure using a novel two-step annealing process. *Sol. Energy* 207, 651–658. <https://doi.org/10.1016/j.solener.2020.07.016>.
- Sigman, M.B., Ghezalbash, A., Hanrath, T., et al., 2003. Solventless synthesis of monodisperse  $\text{Cu}_2\text{S}$  nanorods, nanodisks, and nanoplatelets. *J. Am. Chem. Soc.* 125 (51), 16050–16057. <https://doi.org/10.1021/ja037688a>.
- Tian, Q., Lu, H., Du, Y., Fu, J., et al., 2018. Green atmospheric aqueous solution deposition for high performance  $\text{Cu}_2\text{ZnSn}(\text{S}, \text{Se})_4$  thin film solar cells. *Sol. RRL* 2 (12), 1800233. <https://doi.org/10.1002/solr.201800233>.
- Wang, S., Jiang, Z., Shen, Z., Sun, Y., et al., 2020. Promising Cd-free double buffer layer in CZTSSe thin film solar cells. *Sci. China Mater.* 64, 288–295. <https://doi.org/10.1007/s40843-020-1419-8>.
- Wen, J., Huang, H., Yu, X., Wang, D., et al., 2021. Thermoelectric properties of p-Type  $\text{Cu}_3\text{VSe}_4$  with high seebeck coefficients. *J. Alloys Compd.* 879, 160387 <https://doi.org/10.1016/j.jallcom.2021.160387>.
- Wu, M., Li, Q., Cheng, S., Yao, K., et al., 2022. Cu-V bimetallic selenide with synergistic effect for high-rate and long-life sodium storage. *J. Mater. Res.* 37, 3308–3317. <https://doi.org/10.1557/s43578-022-00623-0>.
- Xin, H., Vorpahl, S.M., Collord, A.D., Braly, I.L., Hillhouse, H.W., 2015. Lithium-doping inverts the nanoscale electric field at the grain boundaries in  $\text{Cu}_2\text{ZnSn}(\text{S}, \text{Se})_4$  and increases photovoltaic efficiency. *Phys. Chem. Chem. Phys.* 17 (37), 23859. <https://doi.org/10.1039/C5CP04707B>.
- Xue, X., Chen, R., Song, X., Tao, A., et al., 2021. Electrochemical  $\text{Mg}^{2+}$  displacement driven reversible copper extrusion/intrusion reactions for high-rate rechargeable magnesium batteries. *Adv. Funct. Mater.* 31 (10), 2009394. <https://doi.org/10.1002/adfm.202009394>.
- Yang, W., Ji, Y., Chen, W., Pan, Y., et al., 2024. The multiple roles of Na ions in highly efficient CZTSSe solar cells. *Small*, 2307807. <https://doi.org/10.1002/sml.202307807>.
- Yang, Y., Wang, G., Zhao, W., et al., 2015. Solution-processed highly efficient  $\text{Cu}_2\text{ZnSnSe}_4$  thin film solar cells by dissolution of elemental Cu, Zn, Sn, and Se powders. *ACS Appl. Mater. Interfaces* 7 (1), 460–464. <https://doi.org/10.1021/am5064926>.
- Yang, Y., Kang, X., Huang, L., Wei, S., Pan, D., 2016. A general water-based precursor solution approach to deposit earth abundant  $\text{Cu}_2\text{ZnSn}(\text{S}, \text{Se})_4$  thin film solar cells. *J. Power Sources* 313, 15–20. <https://doi.org/10.1016/j.jpowsour.2016.01.085>.
- Yin, K., Xu, X., Wang, M., Zhou, J., 2022. A high-efficiency (12.5 %) kesterite solar cell realized by crystallization growth kinetics control over aqueous solution based  $\text{Cu}_2\text{ZnSn}(\text{S}, \text{Se})_4$ . *J. Mater. Chem. A* 10, 779–788. <https://doi.org/10.1039/D1TA09024K>.
- Zhai, X.P., Ma, B., Xiao, M.J., Shang, W., et al., 2023. Flexible optical limiters based on  $\text{Cu}_3\text{VSe}_4$  nanocrystals. *Nanoscale* 15 (25), 10606–10613. <https://doi.org/10.1039/D3NR00498H>.
- Zhang, X., Fu, E., Wang, Y., Zhang, C., 2019. Fabrication of  $\text{Cu}_2\text{ZnSnS}_4$  (CZTS) nanoparticle inks for growth of CZTS films for solar cells. *Nanomaterials* 9 (3), 336. <https://doi.org/10.3390/nano9030336>.

Zhang, X., Tang, Y., Wang, Y., Shen, L., Gupta, A., Bao, N., 2020. Simple one-pot synthesis of  $\text{Cu}_4\text{SnS}_4$  nanoplates and temperature-induced phase transformation mechanism. *CrystEngComm* 22, 1220–1229. [https://doi.org/10.1039/C9CE01772-K](https://doi.org/10.1039/C9CE01772K).

Zhao, X., Pan, Y., Zuo, C., Zhang, F., Huang, Z., et al., 2021a. Ambient air-processed  $\text{Cu}_2\text{ZnSn}(\text{S}, \text{Se})_4$  solar cells with over 12 % efficiency. *Sci. Bull.* 66 (9), 880–883. <https://doi.org/10.1016/j.scib.2020.12.030>.

Zhao, Y., Zhao, X., Kou, D., Zhou, W., et al., 2021b. Local Cu component engineering to achieve continuous carrier transport for enhanced kesterite solar cells. *ACS Appl. Mater. Interfaces* 13 (1), 795–805. <https://doi.org/10.1021/acsami.0c21008>.